Dyes and Pigments 97 (2013) 278–285

Contents lists available at SciVerse ScienceDirect

Dyes and Pigments

journal homepage: www.elsevier.com/locate/dyepig

Synthesis, crystal structure and third-order nonlinear optical properties in the near-IR range of a novel stilbazolium dye substituted with flexible polyether chains

Dandan Li, Daohui Yu, Qiong Zhang, Shengli Li, Hongping Zhou, Jieying Wu*, Yupeng Tian*

Department of Chemistry, Key Laboratory of Functional Inorganic Materials Chemistry of Anhui Province, Anhui University, Hefei 230039, PR China

ARTICLE INFO

Article history:
Received 18 October 2012
Received in revised form
2 January 2013
Accepted 3 January 2013
Available online 16 January 2013

Keywords:
Stilbazolium
Flexible chains
Third-order nonlinear optical properties
Two-photon absorption
Z-scan measurements
Near-infrared laser

ABSTRACT

A novel stilbazolium salt with flexible chains, trans- [4-[*N*,*N*-*bis*(2-(2-methoxyethoxy)ethyl)amino] styryl]-*N*-methylpyridinium tetraphenylborate, was designed, synthesized and fully characterized. Third-order nonlinear optical properties for the new stilbazolium salt have been explored. The results show that the novel dye possesses very large values of the real part of the cubic hyperpolarizability $\chi^{(3)}$, up to 10^{-12} esu, and displays maximum two-photon absorption cross sections within the narrow wavelength range from 950 to 960 nm, while out of the range, it shows a large real part of $\chi^{(3)}$, which was determined by two-photon induced fluorescence and open/closed aperture Z-scan measurements using femtosecond pulse laser in near-infrared range, respectively.

1. Introduction

Molecular materials with nonlinear optical (NLO) properties have been the focus of intense current research. Such materials are of great scientific and technologic interest not only for applications as devices as signal processing, ultrafast optical communication, data storage, optical limiting, logic devices, all-optical switching, and bioimaging, but also for the fundamental understanding of how soft matter interacts with light [1–7]. Research advances in this field depend critically on the development of new materials with strong NLO response. Therefore significant effort has been devoted to building novel NLO molecules. Stilbazolium salts are the best studied amongst such materials and are particularly attractive for device applications [8,9].

It was previously studied by Marder's group that *trans*-4′-(dimethylamino)-*N*-methyl-4-stilbazolium tosylate (DAST) exhibits very pronounced bulk quadratic NLO activity [10]. Then a series of *N*-aryl stilbazolium salts possessing quadratic NLO properties were systematically investigated by Coe's group [11,12]. Recently, efficient TPP (two-photon pumped) lasing has been reported in some *p*-aminostyrylpyridinium dyes that synthesized by Prasad's group [13] and by us [14–17]. Earlier work on NLO materials has established that increasing the internal charge transfer and dimensionality of the molecule, extending π-conjugated system, and assembling inorganic metal ions with organic units which will improve the NLO response. Recently, new chromophore design included tuning the molecular bond length alternation characteristics, introducing electron-rich and electron-deficient hetero-cyclic bridges were proposed, which act as auxiliary donors and acceptors, into the molecular skeleton. Those are different from previous NLO strategies. Very recently, a new chromophore was designed and synthesized to promote the advances in the field of molecular materials with NLO activity by Prasad's group [18].

In this context, we launched a program aimed in the purpose of developing soluble dye in high polar solvents, which shows a negative solvatochromism and the longest excited-state lifetime in water. Furthermore, it exhibits peak intense two-photon fluorescence-emission within narrow wavelength range, and large values of the real part of the cubic hyperpolarizability $\chi^{(3)}$. For another reason, as we know, organic dyes are extensively used as the signaling units in chemosensor design because of their intense absorption and emission properties, which are sensitive to external inputs [19]. In this work, we introduced two methoxyethoxyethyl

* Corresponding authors. Tel.: +86 551 5108151; fax: +86 551 5107342.
E-mail address: yptian@ahu.edu.cn (Y. Tian).

0143-7208/$ – see front matter © 2013 Elsevier Ltd. All rights reserved.
http://dx.doi.org/10.1016/j.dyepig.2013.01.001

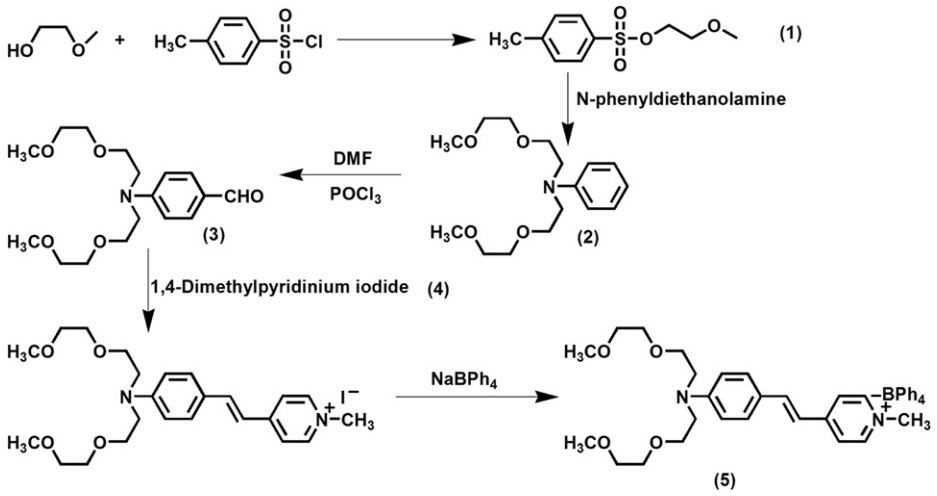

Fig. 1. Synthesis of **5**.

groups into the molecular skeleton, which may provide the possibility for acting as an ion probe or sensing to polarity of the solvents.

2. Experiments

2.1. General

All chemicals used were of analytical grade and the solvents were purified by conventional methods before use. The ^{1}H-NMR spectra were performed on Bruker 400 MHz spectrometer with TMS as the internal standard, coupling constants J are given in Hertz. Elemental analysis was performed on Perkin–Elmer 240 instrument. Mass spectra were determined with a Micromass GCT-MS (ESI source) and MALDI-TOF-MS. IR spectra were recorded on NEXUS 870 (Nicolet) spectrophotometer in the 400–4000 cm^{-1} region using a powder sample on a KBr plate.

Single-crystal X-ray diffraction measurements were carried out on a Bruker Smart 1000 CCD diffractometer equipped with a graphite crystal monochromator situated in the incident beam for data collection at room temperature. The determination of unit cell parameters and data collections were performed with MoK_α radiation (λ = 0.71073 Å). Unit cell dimensions were obtained with least-squares refinements, and all structures were solved by direct methods using SHELXL-97. All non-hydrogen atoms were refined anisotropically. The hydrogen atoms were added theoretically and not refined. The final refinement was performed by full-matrix least-squares methods with anisotropic thermal parameters for non-hydrogen atoms on F^2.

Electronic absorption spectra were obtained on a UV-265 spectrophotometer. Fluorescence measurements were performed using a Hitachi F-7000 fluorescence spectrophotometer.

The TD-DFT {B3LYP[LANL2DZ]} calculations were performed on the optimized structure. All calculations were performed with the G03 software, the TDDFT calculation of the lowest 25 singlet–singlet excitation energies were calculated with a basis set composed of 6–31 G(d,p) for C N H O atoms.

For time-resolved fluorescence measurements, the fluorescence signals were collimated and focused onto the entrance slit of a monochromator with the output plane equipped with a photomultiplier tube (HORIBA HuoroMax-4P). The decays were analyzed by 'least-squares'. The quality of the exponential fits was evaluated by the goodness of fit (χ^2).

TPEF spectra were measured using femtosecond laser pulse and Ti:sapphire system (680–1080 nm, 80 MHz, 140 fs, Chameleon II) as the light source. All measurements were carried out at room temperature.

5 was synthesized by the following reactions (shown in Fig. 1).

2.2. Synthesis

2.2.1. 2-Methoxyethyl-4-methylbenzenesulfonate (1)

A solution of 2-methoxyethanol (7.36 mL, 0.10 mol) and a catalytic amount of TBAB (tetra-*n*-butylammonium bromide) in dichloromethane was stirred, and subsequently NaOH (aq., 30%, 15 mL) was added. A solution of *p*-toluenesulfonyl chloride in dichloromethane was added dropwise. The mixture was stirred for 24 h at room temperature, and then washed with distilled water three times. The product was dried over Na_2SO_4, the solvent was removed under reduced pressure to give a yellow oil. Yield 95%. IR (KBr, cm^{-1}) selected bands: 3468 (m), 2938 (s), 2889 (s), 1597 (m), 1455 (m), 1357 (s), 1184 (s), 1130 (m), 1101 (m), 1018 (m), 919 (m),

Table 1
Crystal data and structure refinement for **5**.

Empirical formula	$C_{48}H_{55}BN_2O_4$
Formula weight	734.75
Temperature	298(2) K
Wavelength	0.71069 Å
Crystal system, space group	Monoclinic, $P2_1/n$
Unit cell dimensions	a = 11.498(5) Å
	b = 20.358(5) Å
	c = 18.085(5) Å
	β = 97.436(5)°
Volume	4198(2) Å^3
Z, Calculated density	4, 1.163 mg/m^3
Absorption coefficient	0.073 mm^{-1}
F(000)	1576
Crystal size	0.30 × 0.20 × 0.20 mm
Theta range for data collection	1.51–25.00°
Limiting indices	$-12 \le h \le 13$, $-21 \le k \le 23$, $-16 \le l \le 16$
Reflections collected/unique	24445/6565 [R(int) = 0.0610]
Completeness to theta = 25.00	88.8%
Absorption correction	None
Max. and min. transmission	0.9856 and 0.9785
Refinement method	Full-matrix least-squares on F^2
Data/restraints/parameters	6565/0/499
Goodness-of-fit on F^2	1.031
Final R indices [I > 2sigma(I)]	R_1 = 0.0604, wR_2 = 0.1564
Largest diff. peak and hole	0.233 and −0.202 e. Å^{-3}

Table 2
Selected bond lengths (Å) and angles (°) of **5**.

N_2–C_{13}	1.368(4)
N_2–C_{15}	1.463(4)
N_2–C_{20}	1.455(4)
C_6–C_7	1.445(4)
C_7–C_8	1.338(4)
C_8–C_9	1.442(4)
C_{13}–N_2–C_{15}	121.0(3)
C_{13}–N_2–C_{20}	121.7(3)
C_{20}–N_2–C_{15}	117.3(3)

821 (m). ^{1}H-NMR (400 MHz, CD_3COCD_3): 3.20 (s, 3H), 3.48 (t, J = 4.6 Hz, 2H), 4.08 (t, J = 4.6 Hz, 2H), 7.71 (d, J = 8.4 Hz, 2H), 7.28 (d, J = 8.4 Hz, 2H), 2.36 (s, 3H). Anal. Calc. for $C_{10}H_{14}SO_4$: C, 52.16; H, 6.13. Found: C, 52.09; H, 6.17.

2.2.2. *N,N-Bis(2-(2-methoxyethoxy)ethyl)benzen amine* ***(2)***

A solution of *N*-phenyldiethanolamine (1.81 g, 0.01 mol) in acetonitrile was slowly dropped into a solution of NaH (0.48 g, 0.02 mol) in acetonitrile, then **1** (4.60 g, 0.02 mol) was added dropwise. The reaction mixture was stirred and refluxed for 24 h at 85 °C. The suspension was filtered, washed with acetonitrile, and the filtration containing product was obtained. The product obtained after evaporation under reduced pressure was purified by silica gel chromatography column using petroleum/ethylacetate (6:1 v/v). Light yellow oil product **2** was collected. Yield 70%. IR (KBr, cm^{-1}) selected bands: 3436 (m), 2921 (s), 1599 (m), 1505 (m), 1459 (m), 1379 (m), 1195 (m), 1117 (m), 752 (m), 686 (m). ^{1}H-NMR (400 MHz, CD_3COCD_3): 3.32 (s, 6H), 3.59 (t, J = 5.2 Hz, 8H), 3.50 (t, J = 4.6 Hz, 4H), 3.65 (t, J = 6 Hz, 4H), 6.75 (d, J = 8.4 Hz, 2H), 7.18 (t, J = 8.0 Hz, 2H), 6.63 (t, J = 7.2 Hz, 1H). MALDI-TOF: *m*/*z*, cal: 297.25, found: 297.39 (M^+). Anal. Calc. for $C_{16}H_{27}NO_4$: C, 64.62; H, 9.15; N, 4.71. Found: C, 64.43; H, 9.50; N, 4.87.

2.2.3. *4-(Bis(2-(2-methoxyethoxy)ethyl)amino)benzaldehyde* ***(3)***

$POCl_3$ (1.84 g, 0.05 mol) was slowly dropped into a dry 100 mL flask which contained 0.73 g (0.01 mol) DMF in ice bath. The mixture was stirred vigorously while a solution of **2** (3.00 g, 0.01 mol) in chloroform (25 mL) was added dropwise, the reaction mixture was stirred and heated under reflux for 15 h at 65 °C and then cooled to room temperature, and then the residue was poured into 500 mL ice water slowly. The NaOH solution was added to adjust the pH of the solution under vigorous stirring. After the pH in the solution had reached 8.0, the mixture was extracted by dichloromethane and dried over by Na_2SO_4. The product obtained after evaporation under reduced pressure was purified by silica gel chromatography column using petroleum/ethylacetate (3:1 v/v). Yellow oil product **3** was collected. Yield 80%. IR (KBr, cm^{-1}) selected bands: 3494 (m), 2877 (s), 2726 (m), 1667 (m), 1596 (s), 1400 (m), 1315 (m), 1170 (m), 1112 (m), 814 (m), 723 (m), 503 (m). ^{1}H-NMR (400 MHz, CD_3COCD_3): 3.30 (s, 6H), 3.71 (t, J = 3.6 Hz, 8H), 3.49 (q, J = 3.8 Hz, 4H), 3.58–3.60 (q, J = 3.8 Hz, 4H), 6.88 (d, J = 9.2 Hz, 2H), 7.70 (d, J = 8.4 Hz, 2H), 9.72 (s, 1H). MALDI-TOF: *m*/*z*, cal: 324.59, found: 324.26 (M^+). Anal. Calc. for $C_{17}H_{52}NO_5$: C, 62.75; H, 8.36; N, 4.30. Found: C, 62.64; H, 8.50; N, 4.37.

2.2.4. *1,4-Dimethylpyridinium iodide* ***(4)***

1,4-Dimethylpyridinium iodide was synthesized according to the literature method [20]. White powder product **4** was collected. Yield 90%. Mp: 155 °C. IR (KBr, cm^{-1}) selected bands: 3451 (m), 3023 (m), 1644 (s), 1517 (m), 1517 (m), 1477 (m), 1289 (s), 1182 (s), 1043 (m), 809 (s), 697 (s), 485 (s). ^{1}H-NMR (400 MHz, d_6-DMSO): 2.61 (3H, s), 4.29 (3H, s), 7.97 (2H, d, J = 6.4 Hz), 8.84 (2H, d, J = 6.4 Hz); M^+(MS/ESI), 108.48.

2.2.5. *Trans-**[**4-[N,N-bis(2-(2-methoxyethoxy)ethyl)amino]styryl]-N-methylpyridinium tetraphenylborate* ***(5)***

Using a 100 mL one-necked flask fitted with a stirrer and a condenser, 3.25 g (0.01 mol) of compound **3**, 2.35 g (0.01 mol) of compound **4**, and 30 mL of absolute ethanol were mixed. Five drops of piperidine were added to the mixture. Then the solution was heated to reflux for 4 h. After cooling, 3.46 g (0.01 mol) of sodium tetraphenylborate was added into the solution. The solution again

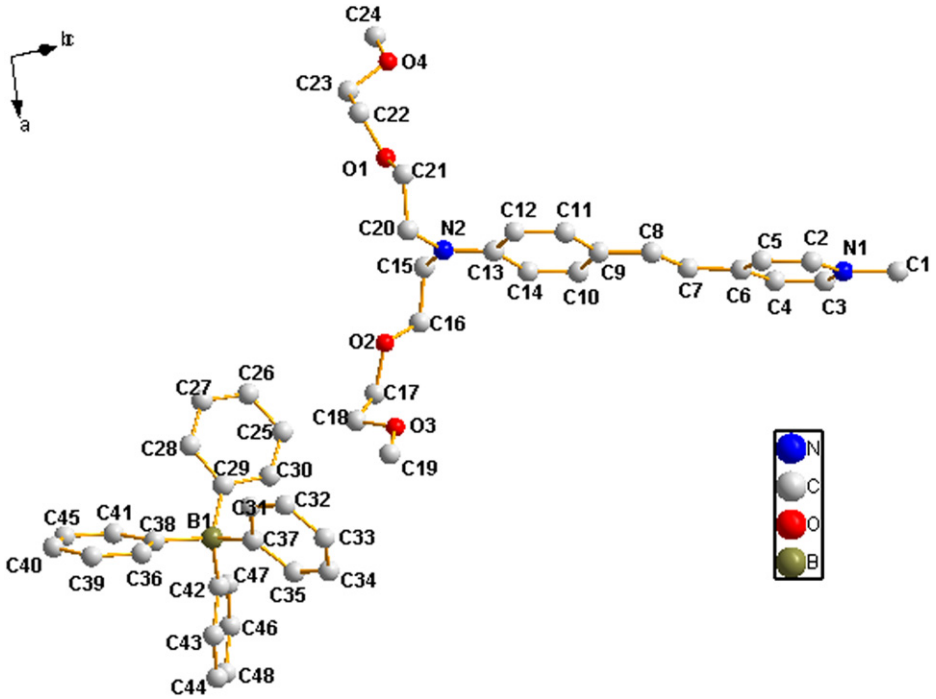

Fig. 2. Crystal structure of **5**. Hydrogen atoms are omitted for clarity.

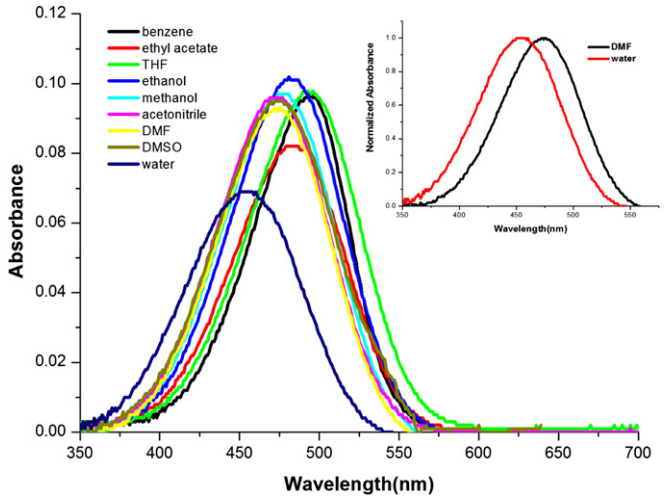

Fig. 3. Linear absorption ($c = 2 \times 10^{-6}$ mol L^{-1}) spectra of **5** in different solvents.

was heated to reflux for 10 min. A red solid formed after cooling. The solution was filtered, and the solid was washed twice with ethanol and water, respectively. Red solid product **5** was collected. Mp: 130 °C. FT-IR (KBr, cm^{-1}) v: 707 (m), 1175 (s), 1523 (m), 1585 (s), 1644 (w), 3063 (w), 2981 (w), 2924 (w), 2891 (w). ^{1}H-NMR (400 MHz, CD_3COCD_3): 8.36 (d, $J = 6.4$ Hz, 2H), 7.89 (d, $J = 6.8$ Hz, 2H), 7.83 (d, $J = 16.0$ Hz, 1H), 7.58 (d, $J = 8.8$ Hz, 2H), 7.36 (m, 9H), 7.11 (d, $J = 16.4$ Hz, 1H), 6.93 (t, $J = 7.6$ Hz, 9H), 6.86 (d, $J = 8.8$ Hz, 2H), 6.78 (t, $J = 7.2$ Hz, 4H), 4.16 (s, 3H), 3.69 (s, 8H), 3.58 (t, $J = 5.2$ Hz, 4H), 3.48 (t, $J = 4.0$ Hz, 4H), 3.29 (s, 6H). ^{13}C-NMR (100 MHz, CD_3COCD_3): 164.9, 154.7, 151.5, 144.8, 143.3, 136.9, 131.4, 126.2, 123.2, 117.6, 112.8, 72.7, 72.0, 69.2, 58.9, 51.8, 47.2, 44.1. M^+ (MS/ESI), 415.33. Anal. Calc. for $C_{48}H_{55}BN_2O_4$: C, 78.46; H, 7.54; N, 3.81. Found: C, 78.04; H, 7.50; N, 3.87.

3. Results and discussion

3.1. Structural features

The single crystals of **5**, suitable for the X-ray analysis, were obtained from the slow evaporation of dichloromethane covered with methanol at room temperature. The crystal data collection and refinement parameters are listed in Table 1. The selected bond distances and angles are given in Table 2. The structure of **5**, together with the atom numbering scheme is shown in Fig. 2. For the molecular structure **5**, the sum of the three C–N–C angles taking nitrogen atom as center (C_{13}–N_2–C_{20}, 121.7(3)°; C_{13}–N_2–C_{15}, 121.0(3)°; C_{20}–N_2–C_{15}, 117.3(3)°) is 360.0°, therefore the trigonal NC_3 is practically coplanar. The least-square plane calculations show that the dihedral angle between the benzene ring and pyridine ring is 13.5°, indicating they are nearly coplanar. It can be seen from Table 2 that all the bond lengths of C–C are located between the normal C=C double bond (1.32 Å) and C–C single bond (1.53 Å), which show that there is a highly π-electron delocalized system in the molecule, which is the necessary condition for it bearing a strong NLO active.

3.2. Linear absorption properties and TD-DFT studies

Fig. 3 shows the absorption spectra of **5** (2 μM) in different solvents. As can be seen from the Fig. 3, by increasing the polarity of the solvent, the absorption of **5** exhibits a blue shift, from DMF to water (from 470 to 450 nm, respectively). This behavior is attributed to a relatively high polar mesomeric form, which is predominant in the ground state. As a result, the hydrogen bond donating solvents decrease the energy of the ground state, by acting as proton donors, leading to a blue shift of the absorption band [21].

The linear absorption of **5** in different organic solvents features one intense absorption band between 450 and 490 nm with the corresponding molar extinction coefficient (~50,000 M^{-1} cm^{-1}),

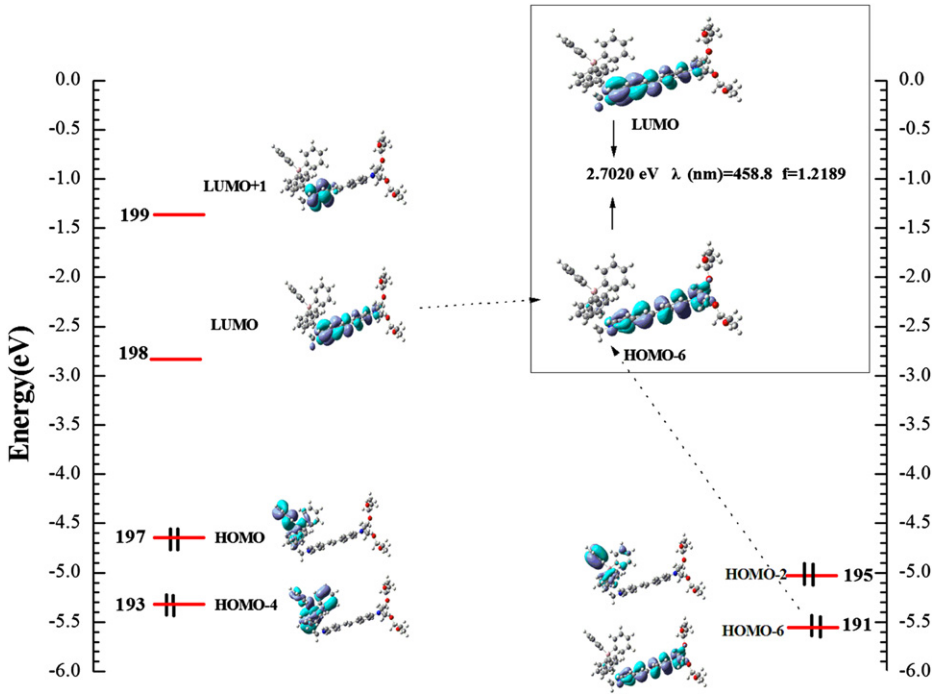

Fig. 4. Molecular orbital energy diagram of **5**.

Table 3
Excitation energy (E), corresponding wavelength (λ), oscillator strength (f) and major contribution of **5**.

E (eV)	λ (nm)	f	Composition (C)	Character
2.7020	458.8	1.2189	191(H-6)->198(0.59508)	ICT

which originates from the $\pi \rightarrow \pi^*$ or intramolecular charge transfer (ICT) transition.

TD-DFT computational studies were performed to elucidate the electronic structures of the ground state of **5**. The schematic representation of the molecular orbitals of **5** was exhibited in Fig. 4, and the energy and composition of ICT are listed in Table 3. The energy band calculated is at 458.86 nm with oscillator strength ($f = 1.2189$). Fig. 4 shows the calculated frontier orbitals of **5**, the energy band was tentatively assigned to ICT. This band mainly originates from transitions of HOMO-6 to LUMO. Therefore the initial DFT and TD-DFT calculations provide reasonable explanations for its absorption spectra.

3.3. One-photon induced fluorescence

The single-photon induced emission spectra of **5** (2 μM) in different solvents are illustrated in Fig. 5. It exhibits a weak fluorescence intensity, which is similar to the other the normal Stilbazolium salts [22,23]. This phenomenon is attributed to that the excited state of **5** is quenched by the anion. The quenching efficiency depends on the chemical nature of the anion and the surroundings [13].

As shown in Fig. 5 (normalized for excitation in benzene and DMSO), one can see that the fluorescence spectra incline to red shift as the solvent polarity increase (566 nm in benzene to 599 nm in DMSO), indicating that the dipole moment of 5 in the excited state is larger than that in the ground state, and an increase in the polarity of the solvent will lower the energy level of the charge transfer excited state [23].

3.4. Quantum yield determination

The fluorescence quantum yields (Φ) were determined using Rh6G as the reference according to the literature method [15]. Quantum yields were corrected as follows:

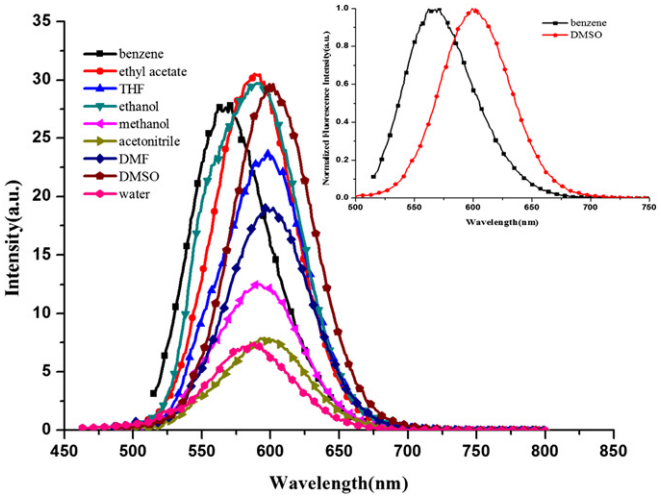

Fig. 5. One-photon induced fluorescence ($c = 2 \times 10^{-6}$ mol L^{-1}) spectra of **5** in different solvents.

Table 4
Single-photon-related photophysical properties of **5** in different solvents.

Solvent	λ_{max}[a] (ε_{max}[b])	λ_{max}[c]	Φ[d]	$\Delta\nu$ (cm^{-1})
Benzene	493(4.95)	566	0.0405	2616
Ethyl acetate	479(4.10)	590	0.0549	3927
THF	490(4.90)	597	0.0373	3657
Ethanol	481(5.25)	589	0.0468	3812
Methanol	474(5.20)	592	0.0187	4205
Acetonitrile	469(4.90)	591	0.0124	4401
DMF	472(5.00)	595	0.0289	4379
DMSO	470(6.00)	599	0.0363	4582
H_2O	450(4.10)	588	0.0139	5215

[a] Peak position of the longest absorption band.
[b] Maximum molar absorbance in 10^4 mol^{-1} L cm^{-1}.
[c] Peak position of SPEF, exited at the absorption maximum.
[d] Quantum yields determined by using Rh6G as standard.

$$\Phi_s = \Phi_r\left(\frac{A_r\eta_s{}^2D_s}{A_s\eta_r{}^2D_r}\right)$$

where the s and r indices designate the sample and reference samples, respectively, A is the absorbance at λ_{exc}, η is the average refractive index of the appropriate solution, and D is the integrated area under the corrected emission spectra [24].

As shown in Table 4, the photophysical properties of **5** show low quantum yield (<10%). The behavior is due to certain nonradiative decay mechanisms that may arise as a result of 'twisted intramolecular charge geometry' (TICT) [25], **5** undergoes an intramolecular transfer of an electron from the donor to the acceptor in the excited state, which is accompanied by a twist around the bond joining the donor and acceptor.

3.5. Fluorescence lifetime

To get more insight into the radiative and nonradiative decay processes, we also conducted time-resolved lifetime experiments.

As shown in Table 5, **5** has a variable excited-state lifetime (50–300 ps) in various solvents. It's worth taking a moment to notice the fact that the fluorescence lifetime in water is the longest. As we know, the fluorescence lifetime is a relatively long process on the time scale of molecular events, and during this time, a high energy fluorophore can undergo a great variety of transformations, ranging from electron redistribution and geometric alteration to reorganization of the surrounding molecules and chemical reactions [26]. In many cases, the energy gained as a result of photon absorption is lost as a nonradiative processes, collectively called quenching [27], and inevitably leads to the decrease of the fluorescence lifetime. From Table 5 we can observe that, with increasing polarity of the solvent, the fluorescence lifetime of **5** decreased, thereby supporting the assumption that because of the nonradiative decay arised as a result of TICT enhancing the quenching efficiency.

3.6. Two-photon excited fluorescence (TPEF)

Detailed experiments reveal that there is no significant linear absorption in the spectral range from 600 to 1200 nm, which indicates that there are no molecular energy levels corresponding to

Table 5
Fluorescence lifetime of **5** in different solvents.

Solvent	Ethyl acetate	THF	DMF	DMSO	Water
τ/ps[a]	255	242	171	47	293

[a] The fitted fluorescence lifetime.

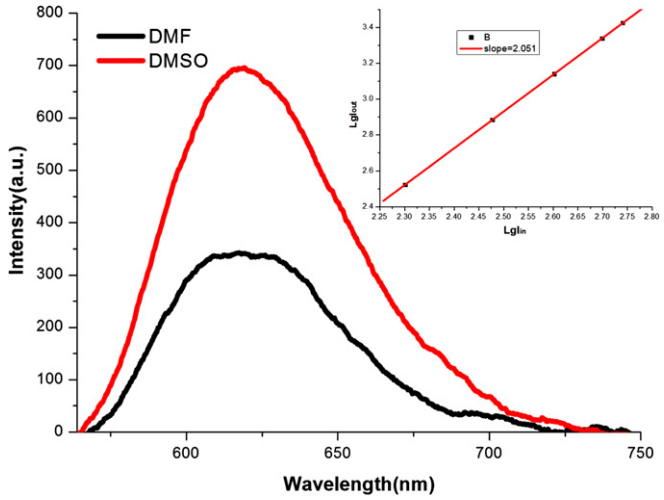

Fig. 6. The two-photon fluorescence spectra of **5** in DMF and DMSO ($c = 1.0 \times 10^{-3}$ mol L^{-1}). Insert figure: Output fluorescence (I_{out}) vs. the square of input laser power (I_{in}) for **5** excitation carried out at 960 nm, with $c = 1.0 \times 10^{-3}$ mol L^{-1} in DMSO.

an electron transition in the spectral range. Therefore, upon excitation from 600 to 1200 nm, it is impossible to produce single-photon-excited up-converted fluorescence. The linear dependence on the square of input laser power suggests a two-photon excitation mechanism at 960 nm for **5** (as an insert figure in Fig. 6).

The two-photon excited fluorescence spectra of **5** were investigated in two organic solvents (Fig. 6, $c = 1.0 \times 10^{-3}$ mol L^{-1}), upon excitation at the optimal wavelength (960 nm), the TPEF spectra of **5** are presented. From Fig. 7 one can see that a two-photon-excited fluorescence band appears about 30 nm red-shifted as compared to its single-photon counterpart. This is due to the re-absorption effect of **5** solution at high concentration [28].

In addition, a majority of the biological samples possess intrinsic florescence due to molecules which are inherently fluorescent and absorb in the ultraviolet and visible region [29]. In our case, the studied **5** can be excited using an IR beam (960 nm) and emit efficiently in the visible region (620 nm) of the spectrum. This is the most attractive feature of the dye for its utility as a biological probe [30].

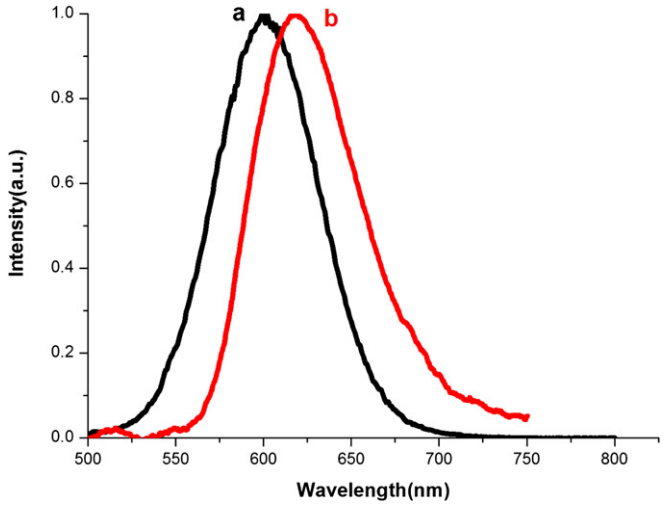

Fig. 7. (a) One-photon excited fluorescence spectrum of **5** in DMSO ($c = 2 \times 10^{-6}$ mol L^{-1}), (b) Two-photon excited fluorescence spectrum of **5** in DMSO ($c = 1.0 \times 10^{-3}$ mol L^{-1}).

3.7. TPA cross-sections

The two-photon absorption (TPA) cross-section σ was measured by comparing the TPEF (two-photon excited fluorescence) intensity of the sample with that of a reference compound by the following equation:

$$\delta = \delta_{ref}\frac{\Phi_{ref}}{\Phi}\frac{c_{ref}}{c}\frac{n_{ref}}{n}\frac{F}{F_{ref}}$$

Here, the subscripts ref stands for the reference molecule (Rh6G). Φ is the quantum yield, n is the refractive index, F is the integrated area under the corrected emission spectrum, c is the concentration of the solution in mol L^{-1}. The δ_{ref} value of reference was taken from the literature [31].

As shown in Fig. 8, two-photon absorption cross sections (δ) of **5** were measured in the wide wavelength range from 800 to 1000 nm. The maximum values in DMF and DMSO are 517 and 668 GM, respectively. Interestingly, from these data, it can be observed that the dramatically larger two-photon absorption cross sections appear in the narrow pathlength about 950–970 nm. This is very different in comparison to previous results [32–37]. Clearly, the present structural modifications can result in pronounced differences in the absorption cross section. Therefore, it is tentatively suggested that there are excited-states (S_1–S_n) distributing in a much narrow energy band [38].

3.8. TPA coefficient β and $\chi^{(3)}$

To further confirm the TPA performances, the TPA coefficient β and $\chi^{(3)}$ of **5** were measured by the Z-scan technique [39,40]. Z-scan is one of the commonly utilized methods to perform $\chi^{(3)}$ measurements. The advantage of this method is that both the real and imaginary parts of $\chi^{(3)}$ can be determined simultaneously or consecutively, using the so-called closed-aperture and open-aperture conditions, respectively. In the present experiments, a 1×10^{-3} M solution of **5** in DMSO contained in a 1.0 mm pathlength quartz cell for Z-scan measurements was performed separately at 920, 960 and 1000 nm wavelengths.

The TPA coefficient β and $\chi^{(3)}$ calculation method can be obtained according to literature methods [18,41]. Fig. 9A–C shows the normalized transmittance plotted as a function of the sample position (z) measured by using open aperture and closed aperture Z-scan technique at 920, 960 and 1000 nm, respectively. Table 6

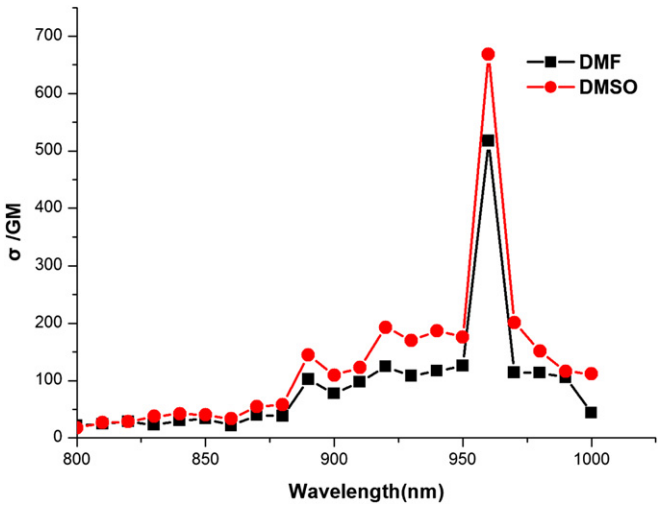

Fig. 8. Two-photon absorption cross sections of **5** in DMF and DMSO vs. excitation wavelengths of identical energy of 0.500 W.

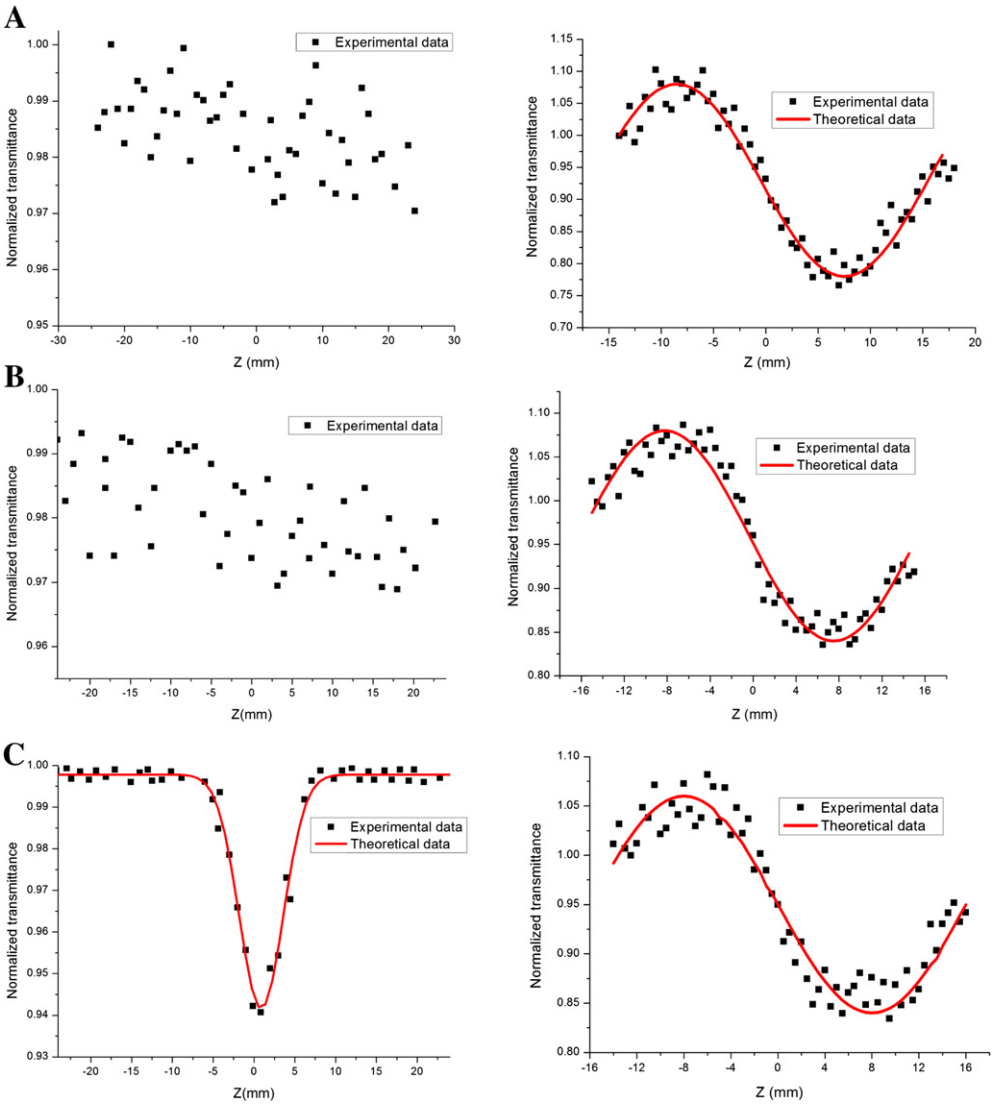

Fig. 9. A. Normalized open-aperture (left) and closed-aperture (right) Z-scan transmittance of **5** in DMSO (0.001 M) at 920 nm. B. Normalized open-aperture (left) and closed-aperture (right) Z-scan transmittance of **5** in DMSO (0.001 M) at 960 nm. C. Normalized open-aperture (left) and closed-aperture (right) Z-scan transmittance of **5** in DMSO (0.001 M) at 1000 nm.

shows the third-order nonlinearity parameters of **5**. From these data, it can be seen that **5** exhibits a large nonlinear refractive index coefficient and possesses very large values of the real part of the cubic hyperpolarizability $\chi^{(3)}$ at 920 and 1000 nm, respectively. However, no TPA was observed under the same conditions. The results are in good agreement with those determined by two-photon-induced fluorescence measurement technique.

Table 6
Open- and closed-aperture Z-scan measurement data for the third-order nonlinearity parameters of **5**.

Wavelength	920 nm	960 nm	1000 nm
n_2 extrapolated to solute (cm^2/W)	4.08×10^{-10}	4.29×10^{-10}	1.45×10^{-10}
Re ($\chi^{(3)}$) extrapolated to solute (esu)	2.26×10^{-12}	2.38×10^{-12}	8.04×10^{-13}
2PA coefficient α_2 (cm/GW) Extrapolated to solute		0.039	
Two-photon cross section σ (GM)		1368.61	
Im ($\chi^{(3)}$) extrapolated to solute (esu)		1.68×10^{-15}	

4. Conclusions

A new stilbazolium salt with flexible polyether chains, 5, was designed and synthesized. One-photon absorption and emission spectra, the excited-state lifetime, two-photon excited fluorescence behavior have been systematically investigated. The relationships between the structures and photophysical properties of **5** can be understood based on both the experimentally and theoretically. It was found that **5** showed a strong solvent-polarity-dependent fluorescence in the visible region, and its fluorescence lifetime is the longest in water compared to those in the other solvents. Furthermore, it exhibits peak intense two-photon fluorescence emission when excited at the narrow wavelength range of a near-infrared pulse laser and possesses very large values of the real part of the cubic hyperpolarizability $\chi^{(3)}$. The results also suggest how to use the NLO molecular material under selected different

wavelengths. The foregoing behavior should establish the foundation for the development of third-order nonlinear optical molecular materials.

Acknowledgments

This work was supported by a grant for the National Natural Science Foundation of China (51142011, 21071001, 21271003, 21271004), the Natural Science Foundation of Anhui Province (1208085MB22), Ministry of Education Funded Projects Focus on returned overseas scholar. Program for New Century Excellent Talents in University (China), Doctoral Program Foundation of Ministry of Education of China (20113401110004).

Appendix A. Supplementary data

Crystallographic data for the structural analysis have been deposited at the Cambridge Crystallographic Data Center, CCDC-874010 for **5**. Copy of this information may be obtained free of charge via www: http://www.ccdc.cam.ac.uk or from The Director, CCDC, 12 Union Road, Cambridge CB221EZ, UK (fax: +44 1223/336 033; email: deposite@ccdc.cam.ac.uk). Structural factors are available on request from the authors. Supporting information can be found in the web version of this paper. Supplementary data associated with this article can be found, in the online version, at http://dx.doi.org/10.1016/j.dyepig.2013.01.001.

References

[1] He GS, Tan LS, Zheng QD, Prasad PN. Multiphoton absorbing materials: molecular designs, characterizations, and applications. Chem Rev 2008;108:1245–330.
[2] Pawlicki M, Collins HA, Denning RG, Anderson HL. Two-photon absorption and the design of two-photon dyes. Angew Chem Int Ed 2009;48:3244–66.
[3] Therien MJ. How to improve your image. Nature 2009;458:716–7.
[4] Reeve JE, Collins HA, Mey KD, Kohl MM, Thorley KJ, Paulsen O, et al. Amphiphilic porphyrins for second harmonic generation imaging. J Am Chem Soc 2009;131:2758–9.
[5] Hales JM. Design of polymethine dyes with large third-order optical nonlinearities and loss figures of merit. Science 2010;327:1485–8.
[6] Haque SA, Nelson J. Toward organic all-optical switching. Science 2010;327:1466–7.
[7] Sumalekshmy S, Fahrni CJ. Metal-ion-responsive fluorescent probes for two-photon excitation microscopy. Chem Mater 2011;23:483–500.
[8] Li L, Cui HJ, Yang Z, Tao XT, Lin XS, Ye N, et al. Synthesis and characterization of thienyl-substituted pyridinium salts for second-order nonlinear optics. CrystEngComm 2012;14:1031–7.
[9] Lacroix PG, Carmen Munoz M, Gaspar AB, Real JA, Bonhommeau S, Rodriguez V, et al. Synthesis, crystal structures, and solid state quadratic nonlinear optical properties of a series of stilbazolium cations combined with gold cyanide counter-ion. J Mater Chem 2011;21:15940–9.
[10] Marder SR, Perry JW, Schaefer WP. Synthesis of organic salts with large second-order optical nonlinearities. Science 1989;245:626–8.
[11] Coe BJ, Harris JA, Asselberghs I, Clays K, Olbrechts G, Persoons A, et al. Quadratic nonlinear optical properties of N-aryl stilbazolium dyes. Adv Funct Mater 2002;12:110–6.
[12] Coe BJ, Harris JA, Asselberghs I, Wostyn K, Clays K, Persoons A, et al. Quadratic optical nonlinearities of N-methyl and N-aryl pyridinium salts. Adv Funct Mater 2003;13:347–57.
[13] Zheng QD, He GS, Lin TC, Prasad PN. Synthesis and properties of substituted (p-aminostyryl)-1-(3-sulfooxypropyl)pyridinium inner salts as a new class of two-photon pumped lasing dyes. J Mater Chem 2003;13:2499–504.
[14] Zhang XJ, Tian YP, Jin F, Wu JY, Xie Y, Tao XT, et al. Self-assembly of an organic chromophore with Cd-S nanoclusters: supramolecular structures and enhanced. Cryst Growth Des 2005;5:565–70.
[15] Hao FY, Zhang XJ, Tian YP, Zhou HP, Li L, Wu JY, et al. Design, crystal structures and enhanced frequency-upconverted lasing efficiencies of a new series of dyes from hybrid of inorganic polymers and organic chromophores. J Mater Chem 2009;19:9163–9.
[16] Tian YP, Li L, Zhou YH, Wang P, Zhou YH, Wu JY, et al. Design and synthesis of two new two-photon absorbing pyridine salts as ligands and their rare earth complexes. Cryst Growth Des 2009;9:1499–504.
[17] Wu JY, Hu GJ, Wang P, Hao FY, Zhou HP, Zhou AM, et al. Organic/polyoxometalate hybridization dyes: crystal structure and enhanced two-photon absorption. Dye Pigment 2010;88:174–9.
[18] He GS, Zhu J, Baev A, Samo M, Frattarelli DL, Watanabe N, et al. Twisted π-system chromophores for all-optical switching. J Am Chem Soc 2011;13:6675–80.
[19] (a) de Silva AP, Gunaratne HQN, Gunnlaugsson T. Signaling recognition events with fluorescent sensors and switches. Chem Rev 1997;97:1515–66;
(b) Bissell RA, de Silva AP, Gunaratne HQN, Lynch PLM. Molecular fluorescent signaling with fluor-spacer-receptor systems: approaches to sensing and switching devices via supramolecular photophysics. Chem Soc Rev 1992;21:187–95.
[20] Zhao CF, He GS, Bhawalkar JD, Park CK, Prasad PN. Newly synthesized dyes and their polymer/glass composites for one- and two-photon pumped solid-state cavity lasing. Chem Mater 1995;7:1979–83.
[21] Lal M, Levy L, Kim KS, He GS, Wang X, Min YH, et al. Silica nanobubbles containing an organic dye in a multilayered organic/inorganic heterostructure with enhanced luminescence. Chem Mater 2000;12:2632–9.
[22] Zhao CF, Gvishi R, Narang U, Ruland G, Prasad PN. Structures, spectra, and lasing properties of new (aminostyryl)pyridinium laser dyes. J Phys Chem 1996;100:4526–32.
[23] Wang XM, Wang D, Zhou GY, Yu WT, Zhou YF, Fang Q, et al. Symmetric and asymmetric charge transfer process of two-photon absorbing chromophores: bis-donor substituted stilbenes, and substituted styrylquinolinium and styrylpyridinium derivatives. J Mater Chem 2001;11:1600–5.
[24] Gray TG, Rudzinski CM, Meyer EE, Holm RH, Nocera DG. Spectroscopic and photophysical properties of hexanuclear rhenium(III) chalcogenide clusters. J Am Chem Soc 2003;125:4755–70.
[25] Rullière C, Grabowski ZR, Dobkowski J. Picosecond absorption spectra of carbonyl derivatives of dimethylaniline: the nature of the tict excited states. Chem Phys Lett 1987;137:408–13.
[26] Peng XJ, Yang ZG, Wang JY, Fan JL, He YX, Song FL, et al. Fluorescence ratiometry and fluorescence lifetime imaging: using a single molecular sensor for dual mode imaging of cellular viscosity. J Am Chem Soc 2011;133:6626–35.
[27] Berezin MY, Achilefu S. Fluorescence lifetime measurements and biological imaging. Chem Rev 2010;110:2641–84.
[28] Ren Y, Fang Q, Yu WT, Lei H, Tian YP, Jiang MH, et al. Synthesis, structures and two-photon pumpedup-conversion lasing properties of two new organic salts. J Mater Chem 2000;10:2025–30.
[29] Chorvat Jr D, Chorvatova A. Multi-wavelength fluorescence lifetime spectroscopy a new approach to the study of endogenous fluorescence in living cells and tissues. Laser Phys Lett 2009;6:175–93.
[30] Narang U, Zhao CF, Bhawalkar JD, Bright FV, Prasad PN. Characterization of a new solvent-sensitive two-photon-induced fluorescent (aminostyryl) pyridinium salt dye. J Phys Chem 1996;100:4521–5.
[31] (a) Xu C, Webb WW. Measurement of two-photon excitation cross sections of molecular fluorophores with data from 690 to 1050 nm. J Opt Soc Am B 1996;13:481–91;
(b) Albota MA, Xu C, Webb WW. Two-photon fluorescence excitation cross sections of biomolecular probes from 690 to 960 nm. Appl Opt 1998;13:481.
[32] Iwase Y, Kamada K, Ohta K, Kondo K. Synthesis and photophysical properties of new two-photon absorption chromophores containing a diacetylene moiety as the central π-bridge. J Mater Chem 2003;13:1575–81.
[33] Kamada K, Iwase Y, Sakai K, Kondo K, Ohta K. Cationic two-photon absorption chromophores with double- and triple-bond cores in symmetric/asymmetric arrangements. J Phys Chem C 2009;113:11469–74.
[34] Feng XJ, Wu PL, Bolze F, Leung HWC, Li KF, Mak NK, et al. Cyanines as new fluorescent probes for DNA detection and two-photon excited bioimaging. Org Lett 2010;12:2194–7.
[35] Wang XC, Tian XH, Zhang Q, Sun PP, Wu JY, Zhou HP, et al. Assembly, two-photon absorption, and bioimaging of living cells of a cuprous cluster. Chem Mater 2012;24:954–61.
[36] Masanta G, Lim CS, Kim HJ, Han JH, Kim HM, Cho BR. A mitochondrial-targeted two-photon probe for zinc ion. J Am Chem Soc 2011;133:5698–700.
[37] Chen DG, Zhong C, Dong XH, Liu ZH, Qin JG. A new building block, bis(thiophene vinyl)-pyrimidine, for constructing excellent two-photon absorption materials: synthesis, crystal structure and properties. J Mater Chem 2012;22:4343–8.
[38] Johnsen M, Ogilby PR. Effect of solvent on two-photon absorption by vinyl benzene derivatives. J Phys Chem A 2008;112:7831–9.
[39] Sheik-Bahae M, Said AA, Wei TH, Hagan DJ, Van Stryland EW. Sensitive measurement of optical nonlinearities using a single beam. IEEE J Quantum Electron 1990;26:760–9.
[40] Zhao W, Paltty-Muhoray P. Z-scan measurement of $\chi^{(3)}$ using top-hat beams. Appl Phys Lett 1994;65:673–5.
[41] Li SL, Wu JY, Tian YP, Tang YW, Jiang MH, Fun HK. Preparation, characterization, two-photon absorption and optical limiting properties of a novel metal complex containing carbazole. Opt Mater 2006;28:897–903.